Sciencexpress Report

A Fast Soluble Carbon-Free Molecular Water Oxidation Catalyst Based on Abundant Metals

Qiushi Yin,[1] Jeffrey Miles Tan,[1] Claire Besson,[1,2] Yurii V. Geletii,[1] Djamaladdin G. Musaev,[1] Aleksey E. Kuznetsov,[1] Zhen Luo,[1] Ken I. Hardcastle,[1] Craig L. Hill[1*]

[1]Department of Chemistry, Emory University, Atlanta, GA 30322, USA. [2]Institut Parisien de Chimie Moléculaire, UMR CNRS 7201, UPMC Univ. Paris 06, Case 42, 4 place Jussieu, 75005 Paris, France.

*To whom correspondence should be addressed. E-mail: chill@emory.edu

Traditional homogeneous water oxidation catalysts are plagued by instability under the reaction conditions. We report that the complex $[Co_4(H_2O)_2(PW_9O_{34})_2]^{10-}$ (1) comprising a Co_4O_4 core stabilized by oxidatively resistant polytungstate ligands, is a hydrolytically and oxidatively stable homogeneous water oxidation catalyst that self assembles in water from salts of earth abundant elements (Co, W and P). With $[Ru(bpy)_3]^{3+}$ (bpy = 2,2'-bipyridine) as the oxidant, we observe catalytic turnover frequencies for O_2 production $\geq 5\ s^{-1}$ at pH 8. The rate's pH sensitivity reflects the pH dependence of the 4-electron H_2O/O_2 couple. Extensive spectroscopic, electrochemical, and inhibition studies firmly indicate that 1 is stable under catalytic turnover conditions: neither hydrated cobalt ions nor cobalt hydroxide/oxide particles form in situ.

Producing renewable clean energy has become one of the most profound challenges of the 21st century (*1*). Most of the world's current energy supplies come from sunlight converted to chemical energy by plant photosynthesis. A central thrust of the current energy research focuses on artificial photosynthesis (*2, 3*). Despite the intense global efforts to develop viable abiological water splitting systems, breakthroughs are needed in selectivity, speed, and stability of all three operational units: the sensitizer for light absorption and catalysts for water reduction and oxidation. Developing a viable water oxidation catalyst (WOC) has proven particularly challenging (*4*). An effective WOC must be fast, capable of water oxidation at a potential minimally above the thermodynamic value ($H_2O \rightarrow O_2 + 4H^+ + 4e^-$; 1.229–0.059×pH at 25 °C), and, critically, stable to air, water and heat (oxidative, hydrolytic, and thermal stability). There are many research groups working on heterogeneous and homogeneous WOCs. Heterogeneous WOCs generally have the advantages of low cost, ease of interface with electrode systems, and critically, oxidative stability, but they are harder to study and thus optimize than homogeneous catalysts and they tend to deactivate by surface poisoning or aggregation (*5-9*). Recently, Kanan and Nocera reported a robust heterogeneous WOC based on earth abundant cobalt and phosphate (*8*), after earlier work by Creutz and Sutin (*10*), and demonstrated self assembly under turnover conditions, a key to self repair (*11*). More recently the groups of Mallouk (*9*) and Frei (*12*) reported high catalytic water oxidation rates using colloidal IrO_2•nH_2O particles and Co_3O_4 (spinel) particles, respectively. In contrast, homogeneous WOCs are more amenable to spectroscopic, crystallographic, physicochemical, and computational investigation, and thus more readily optimized. In addition, each individual molecule of a homogeneous catalyst is, in principle, capable of doing chemistry (a cost issue when precious metals such as Ru are involved). However, nearly all homogeneous catalysts contain organic ligands that are thermodynamically unstable with respect to oxidative degradation. As a result, all homogenous WOCs with organic ligands reported to date are oxidatively deactivated (*13-23*). A general goal is to realize WOCs that have the stability, durability, and accessibility of heterogeneous metal oxide catalysts with the activity, selectivity and tunability of homogeneous catalysts. To this end a homogeneous polyoxometalate (POM) WOCs with oxidatively-resistant polytungstate units multiply ligating a Ru_4O_4 core was recently reported (*24-26*). This WOC is as fast as reported homogeneous catalysts containing organic ligands, but Ru is neither abundant nor inexpensive and thus very likely prohibitive for use on a realistic scale. Therefore, discovery of a stable and fast homogenous WOC, without organic ligands, based on earth abundant elements would be highly useful.

We report here a homogeneous catalyst, B-type $[Co_4(H_2O)_2(\alpha\text{-}PW_9O_{34})_2]^{10-}$ (**1**), that is free of carbon-based ligands (Fig. 1). It is easily prepared from readily available salts and oxides of earth abundant elements (Co, W and P). To explore POM-stabilized multi-Co-oxide clusters as WOCs, we use the relatively strong and stable stoichiometric oxidant, Tris(2,2'-bipyridyl)triperchlororuthenium(III), (henceforth "$[Ru(bpy)_3]^{3+}$"; eq. 1). The oxygen yield is monitored using gas chromatography by withdrawing gas samples from the reaction vessel headspace (*24, 27*).

$$4\,[Ru(bpy)_3]^{3+} + 2\,H_2O \xrightarrow{WOC} 4\,[Ru(bpy)_3]^{2+} + 4\,H^+ + O_2 \quad (1)$$

We examined eight cobalt-containing POMs as water oxidation catalysts (Table 1A). Only $[Co_4(H_2O)_2(\alpha\text{-}PW_9O_{34})_2]^{10-}$ (**1**) was active. Cyclic voltammetry of 1 mM **1** shows a large catalytic current with a low overpotential for the water oxidation (Fig. 2A). This characteristic feature is not observed for complexes **2** through **8**. Close examination of the studied complexes reveals that all cobalt-containing POMs have different cobalt-core structures than **1** with the exception of $[Co_4(H_2O)_2(P_2W_{15}O_{56})_2]^{16-}$ (**2**) (fig. S11). However, **2** is synthesized and crystallized at a much lower pH than **1** and is also known to be unstable under our catalytic conditions (pH 7.5 to 8.0) (*28*). The total yield of oxygen is always less than 100% based on oxidant due to competing bipyridyl ligand oxidation (*10*). A first-order hyperbolic fit of the O_2-yield to the concentration of **1** is consistent with this description (fig. S1).

The turnover frequency (TOF) for **1** (eq. 1) at pH 8 is > 5 s^{-1}, which compares well to the 0.9 s^{-1} observed for the [Cp*(Cl)Ir(ppy)] WOC recently reported by Brudvig, Crabtree and co-workers (*22*). The rate of water oxidation catalyzed by **1** is highly sensitive to pH. Increasing pH from the initial value of 7.5 to 8.0 (sodium phosphate buffer, NaPi) decreases the reaction time from 270 s to 90 s (respective final pHs after reaction are 7.3 and 7.5). The reaction is faster still in a solution with a higher buffer capacity at pH 8.0 (a mixture of 30 mM NaPi and 30 mM sodium borate buffer; final pH > 7.9). With 1.2×10^{-4} mM **1** and 2.4 mM $[Ru(bpy)_3]^{3+}$, we obtain a TON ~10^3 in under three minutes. Accordingly, the apparent TON also increases sharply at higher pH due to the faster rate of water oxidation. Here, TON is limited by the concentration of the $[Ru(bpy)_3]^{3+}$, which, in turn, is limited by the formation of an insoluble adduct between **1** and $[Ru(bpy)_3]^{3+/2+}$.

As noted above, the cobalt-containing POM, **1**, is undemanding to synthesize. We prepare it in over 35% yield in a one-pot equilibration synthesis as first reported by Weakley *et al* that entails simply heating Co^{2+}, phosphate, and tungstate in a 2:1:9 ratio in water at reflux (*29*). This synthesis of **1** defines a mechanism for self-repair, a strategy used in our previous work (*11*) and in the recent work by Kanan and Nocera on their heterogeneous cobalt phosphate catalyst (*8*). Homogeneous catalysts like **1** utilize discrete molecules in solution for turnover as opposed to only select sites on the surface of most heterogeneous catalysts. This is a likely factor in a far higher observed efficiency of catalytic water oxidation per cobalt atom in the case of **1** relative to the heterogeneous cobalt phosphate catalyst.

Aqueous cobalt ions and cobalt hydroxide/oxides that form *in situ* from the former are both known to be water oxidation catalysts (*6*, *8*, *10*). Thus we now describe seven lines of experimental evidence that **1** is a stable molecular WOC under turnover conditions and does not form either aqueous cobalt ions or cobalt hydroxide/oxide. The first two arguments are that no changes are observed in either the UV/Visible or ^{31}P NMR spectra of a solution of **1** at pH 8 (the pH in the catalytic experiments) over a one month period (fig. S3 and fig. S4C). UV-Vis and ^{31}P NMR spectra also both establish that **1** is stable for at least one day within the pH range of 3.5 to 9 (fig. S4).

The third experimental probe of the stability of **1** involved selective catalyst poisoning experiments using 2,2'-bipyridine (bpy) as an inhibitor (fig. S2). Bpy reacts with $Co(aq)^{2+}$ to form $[Co(bpy)_3]^{2+}$ (*30*), inhibiting all water oxidation activity. In contrast, the addition of the same molar excess of bpy to solutions of **1** has a relatively minor effect on the apparent water oxidation activity (Table 1B). The observed slight decrease in activity can be attributed to bpy competitively coordinating to the cobalt core of **1**, or the irreversible oxidative degradation of bpy, which is proportional to the bpy concentration. Similarly, aging **1** under reaction conditions for 3 days has no effect on its catalytic water oxidation activity (Table 1B), whereas aging $Co(NO_3)_2$ under the same conditions for 3 days significantly decreases its catalytic activity. This observation tracks with well known cobalt hydroxide/oxide formation above neutral pH (*31*), decreasing the effective surface area and catalytic activity. In addition, at pH 6.2, no water oxidation is observed for reactions catalyzed by **1,** whereas $Co(NO_3)_2$ is still capable of catalyzing a small extent of water oxidation (Table 1B). These results are consistent with **1** being the catalytically active species and its polydentate polytungstate ligands preventing formation of cobalt hydroxide/oxide particles.

For our fourth probe of the stability of **1**, we characterized the post-reaction solution containing **1** using ^{31}P NMR despite the low solubility of **1** in the presence of excess $[Ru(bpy)_3]^{2+}$. When [**1**] = 0.015 mM, as few as 40 equivalents of $[Ru(bpy)_3]^{3+/2+}$ (corresponding to a TON of eight to nine) make the post-reaction solution supersaturated, as indicated by the formation of a light yellow precipitate that forms in minutes to hours. To prevent precipitation, we removed $[Ru(bpy)_3]^{2+}$ from the post-reaction solution by adding $NaBPh_4$ and removing solid $[Ru(bpy)_3][BPh_4]_2$ by filtration. In the ^{31}P NMR spectrum of this solution, **1** (1850 ppm, $\Delta\nu_{1/2}$ = 600 Hz) was the only species detected besides the free phosphate originating from the buffer solution, indicating that **1** remains intact under catalytic water oxidation conditions (fig. S5).

The fifth and sixth experimental probes of the stability of **1** involved IR characterization and reuse of the WOC after an initial catalytic run, which we carried out under conditions scaled up by a factor of 19 relative to run #1 in Table 1B. After the reaction was complete, we saturated the solution with $[Ru(bpy)_3]^{2+}$, which acts as a counter-ion for complex **1**, resulting in its precipitation. The infrared spectrum of the precipitate showed the characteristic peaks of **1**, a B-type sandwich polytungstate, $[Co_4(H_2O)_2(PW_9O_{34})_2]^{10-}$, at 1037 cm^{-1}, 939 cm^{-1}, 882 cm^{-1}, and 767 cm^{-1} (fig. S6), indicating that the POM framework remains intact after catalysis. For simplicity, we assumed a 1:1 ratio of the $[Ru(bpy)_3]^{2+}$ and **1** in the precipitate, and assigned the molecular formula of the precipitate to be **$Na_8Ru(bpy)_3$-1**. Applying the corresponding molecular weight, we used *ca.* 0.0032 mM **$Na_8Ru(bpy)_3$-1** as catalyst in the reaction of $[Ru(bpy)_3]^{3+}$ with water in pH 8 NaPi buffer in the presence of bpy. This reaction gave an O_2 yield of 49.3% and a TON of 58 per **1**, exactly reproducing the activity of pure crystalline **Na_{10}-1** (run #2, Table 1B).

The seventh argument for the stability of **1** during catalysis is voltammetric behavior demonstrating that catalytic activity of the active species is retained after turnover. Specifically, we document an electrochemical-chemical mechanism involving **1**: in absence of **1** a conventional voltammogram is observed for the $[Ru(bpy)_3]^{3+}/[Ru(bpy)_3]^{2+}$ couple; however, upon addition of **1**, an increased anodic current peak and decreased cathodic current peak is observed for this couple (Fig. 2B). This indicates the rapid reduction of $[Ru(bpy)_3]^{3+}$ by **1** followed by reduction of the oxidized **1** by water. The observed catalytic current increases with catalyst concentration (*24*). In addition, Fig. 2B compares the current for a freshly prepared solution of $[Ru(bpy)_3]^{2+}$ and **1** (green line) with that for a solution that has already undergone catalytic chemical reduction of an equivalent amount of $[Ru(bpy)_3]^{3+}$ by **1** (blue line). These two catalytic currents match, implying that there is no evident catalyst deactivation and that the concentration of **1** remains constant after catalysis. In contrast, the same cyclic voltammetric experiment using $Co(NO_3)_2$ in place of **1** shows a marked decrease in the catalytic water oxidation current for the solution after chemical water oxidation when compared to that of an analogous solution containing unreacted $[Ru(bpy)_3]^{2+}$ and $Co(NO_3)_2$ (fig. S7). Once again, this finding is consistent with aqueous cobalt hydrolyzing and condensing to hydroxide/oxide particles under oxidative conditions, decreasing the effective catalyst concentration.

Computational studies of the electronic structure of **1** provide additional support for the oxidative stability of the polytungstate ligands. The four top HOMO's of a high-spin ground state **1** are mostly cobalt core orbitals, and there is almost no involvement of tungstate orbitals (fig. S8). These findings indicate that the polytungstate ligands are unlikely to participate in the water oxidation reaction and should be effectively inert under catalytic conditions.

Our reporting of this catalyst establishes d-electron-transition metal oxide clusters stabilized by robust polydentate POM ligands as a compelling class of self-assembling inorganic complexes capable of catalyzing fast water oxidation in a homogeneous medium. This prompts the examination of other POM-stabilized multi-transition-metal oxide cluster molecules involving both other metals (e.g. Fe and Mn) and new POM ligands as candidate WOCs. Moreover, the identification of a molecular Co-based WOC may allow further investigation of its mechanism of action, providing a basis for the understanding of Co-based water oxidation catalysis in general. In addition, **1** may serve as a template for future optimizations of all-inorganic WOCs as well as their incorporation into water splitting systems. No photosensitizers were used in this report. While $[Ru(bpy)_3]^{3+}$ was used as a stoichiometric oxidant in this study in order to demonstrate the water oxidation activity of **1**, it is ultimately desirable to use solar power to accomplish water oxidation. The apparently straightforward use of $[Ru(bpy)_3]^{2+}$ as a photosensitizer, however, might not be optimal given the oxidative instability of this complex. Our future work will focus on the use of **1** in light-driven all-inorganic and other water splitting systems in addition to clarifying its mechanism for water oxidation.

References and Notes

1. J. Chow, R. J. Kopp, P. R. Portney, *Science* **302**, 1528 (2003).
2. N. S. Lewis, D. G. Nocera, *Proc. Nat. Acad. Sci.* **103(43)**, 15729 (2006).
3. V. Balzani, A. Credi, M. Venturi, *ChemSusChem* **1**, 26 (2008).
4. R. Eisenberg, H. B. Gray, *Inorg. Chem.* **47**, 1697 (2008).
5. V. Y. Shafirovich, N. K. Khannanov, V. V. Strelets, *Nouveau J. de Chimie* **4**, 81 (1980).
6. A. Harriman, I. J. Pickering, J. M. Thomas, P. A. Christensen, *J. Chem. Soc. Faraday Trans. 1*, **84**, 2795 (1988).
7. G. L. Elizarova, G. M. Zhidomirov, V. N. Parmon, *Catal. Today* **58**, 71 (2000).
8. M. W. Kanan, D. G. Nocera, *Science* **321**, 1072 (2008).
9. W. J. Youngblood *et al.*, *J. Am. Chem. Soc.* **131**, 926 (2009).
10. P. K. Ghosh, B. S. Brunschwig, M. Chou, C. Creutz, N. Sutin, *J. Am. Chem. Soc.* **106**, 4772 (1984).
11. I. A. Weinstock *et al.*, *Nature* **414**, 191 (2001).
12. F. Jiao, H. Frei, *Angew. Chem. Int. Ed.* **48**, 1841 (2009).
13. S. W. Gersten, G. J. Samuels, T. J. Meyer, *J. Am. Chem. Soc.* **104**, 4029 (1982).
14. T. Wada, K. Tsuge, K. Tanaka, *Angew. Chem. Int. Ed.* **39**, 1479 (2000).
15. J. Limburg *et al.*, *J. Am. Chem. Soc.* **123**, 423 (2001).
16. J. K. Hurst, *Coord. Chem. Rev.* **249**, 313 (2005).
17. R. Zong, R. Thummel, *J. Am. Chem. Soc.* **127**, 12802 (2005).
18. J. T. Muckerman, D. E. Polyansky, T. Wada, K. Tanaka, E. Fujita, *Inorg. Chem.* **47**, 1787 (2008).

19. R. Brimblecombe, G. F. Swiegers, G. C. Dismukes, L. Spiccia, *Angew. Chem. Int. Ed.* **47**, 7335 (2008).
20. S. Romain, F. Bozoglian, X. Sala, A. Llobet, *J. Am. Chem. Soc.* **131**, 2768 (2009).
21. S. W. Kohl *et al.*, *Science* **324**, 74 (2009).
22. J. F. Hull *et al.*, *J. Am. Chem. Soc.* **131**, 8730 (2009).
23. H. Kunkely, A. Vogler, *Angew. Chem. Int. Ed.* **48**, 1685 (2009).
24. Y. V. Geletii *et al.*, *Angew. Chem. Int. Ed.* **47**, 3896 (2008).
25. A. Sartorel *et al.*, *J. Am. Chem. Soc* **130**, 5006 (2008).
26. Y. V. Geletii *et al.*, *J. Am. Chem. Soc.* **131**, 7522 (2009).
27. Materials and methods are available as supporting material on *Science* Online.
28. L. Ruhlmann, L. Nadjo, J. Canny, R. Contant, R. Thouvenot, *Eur. J. Inorg. Chem.*, 975 (2002).
29. T. J. R. Weakley, H. T. Evans, Jr., J. S. Showell, G. F. Tourné, C. M. Tourné, *J. Chem. Soc. Chem. Comm.* **4**, 139 (1973).
30. F. H. Burstall, R. S. Nyholm, *J. Chem. Soc.*, 3570 (1952).
31. J. Baes, Charles F., R. E. Mesmer, *The Hydrolysis of Cations*. (John Wiley & Sons, New York, 1976), pp. 489.
32. We thank the U.S. Department of Energy through Grant DE-FG02-03ER-15461 for support of this work. Dr. Claire Besson thanks the French MENRT for a research fellowship. Additional details on the crystal structure investigations may be obtained from the Fachinformationszent Wrum Karlsruhe, 76344 Eggenstein-Leopoldshafen, Germany, on quoting registry number CSD-421465.

Supporting Online Material
www.sciencemag.org/cgi/content/full/science.1185372/DC1
Materials and Methods
Figs. S1 to S11
References

01 December 2009; accepted 25 February 2010
Published online 11 March 2010; 10.1126/science.1185372
Include this information when citing this paper.

Fig. 1. X-ray structure of **Na_{10}-1** in combined polyhedral ($[PW_9O_{34}]$ ligands) and ball-and-stick (Co_4O_{16} core) notation. Co: purple, O/OH_2(terminal): red; PO_4: orange tetrahedra; WO_6: gray octahedra. Hydrogen atoms, water molecules and sodium cations are omitted for clarity.

Fig. 2. (A) Cyclic voltammogram (CV) of 50 mM sodium phosphate solution at pH 8 without **1** (black curve) and with 1 mM **1** (red curve). **(B)** Cyclic voltammogram of aqueous 0.857 mM $[Ru(bpy)_3]^{2+}$ alone (red), 3.2 μM **1** alone (black), 0.857 mM $[Ru(bpy)_3]^{2+}$ combined with 3.2 μM **1** (green) or 1.6 μM **1** (yellow), and a post-reaction solution in which initially dissolved 0.857 mM $[Ru(bpy)_3]^{3+}$ has been reduced through water oxidation catalyzed by 3.2 μM **1** (blue). The series of CVs for 0 μM **1** (red), 1.6 μM **1** (yellow), and 3.2 μM **1** (green) added to 0.857 mM $[Ru(bpy)_3]^{2+}$ shows increasing anodic current and decreasing cathodic current, demonstrating the correlation between increasing catalytic current and the concentration of **1**. Conditions: 60 mM NaPi, pH 8, scan rate 25 mV/s; potentials measured and reported versus an Ag/AgCl reference electrode.

Table 1. Catalytic water oxidation by soluble complexes. Reactions were run in 30 mM NaPi buffer, initial pH 8.0 unless otherwise stated, 1.5 mM $[Ru(bpy)_3](ClO_4)_3$, ambient temperature; bpy = 2,2'-bipyridine; turnover number, TON = $n_{O2}/n_{catalyst}$;

O_2-yield = $\frac{4n_{O_2}}{n_{Ru(bpy)_3}}$.

(A) Polyoxometalate (POM) systems.

Complex	Complex concentration (mM)	bpy (mM)	TON	O_2 yield (%)
$[Co_4(H_2O)_2(PW_9O_{34})_2]^{10-}$ (**1**)	0.0032	0.06	75	64
$[Co_4(H_2O)_2(P_2W_{15}O_{56})_2]^{10-}$ (**2**)	0.0064	0.06	0	0
$[Co(H_2O)PW_{11}O_{39}]^{5-}$ (**3**)	0.0064	0.06	0	0
$[Co(H_2O)SiW_{11}O_{39}]^{6-}$ (**4**)	0.0064	0.06	0	0
$[Co_3(H_2O)_3(PW_9O_{34})_2]^{12-}$ (**5**)	0.0064	0.06	0	0
$[Co_3(H_2O)_3SiW_9O_{37}]^{10-}$ (**6**)	0.0064	0.06	0	0
$[WCo_3(H_2O)_2(CoW_9O_{34})_2]^{12-}$ (**7**)	0.0064	0.06	0	0
$[Co_7(H_2O)_2(OH)_2P_2W_{25}O_{94}]^{16-}$ (**8**)	0.0064	0.06	0	0

(B) The effect of bpy on the catalytic water oxidation activity of **1** and $Co(aq)^{2+}$.

Run	Complex	Complex concentration (mM)	bpy (mM)	Buffer	TON	O_2 yield (%)
1	**1**	0.0032	0	pH 8 NaPi	78.1	66.7
2	**1**	0.0032	0.3012	pH 8 NaPi	56	48
3	$Co(NO_3)_2$	0.013*	0.3012	pH 8 NaPi	0	0
4	$Co(NO_3)_2$	0.060†	0.3012	pH 8 NaPi	0.2	<4
5	$Co(NO_3)_2$	0.013	0	pH 8 NaPi	23.4	80
6	no catalyst	--	0	pH 8 NaPi	0	0
7	**1**	0.0032	0	pH 6.2 NaPi/phthalic acid‡	0	0
8	$Co(NO_3)_2$	0.013	0	pH 6.2 NaPi/phthalic acid	10	35
9	**1**	0.0032	0.135	pH 8 NaPi	70.3	60
10	**1** (aged)§	0.0032	0.135	pH 8 NaPi	71.2	60.8
11	$Co(NO_3)_2$ (aged)§	0.013	0	pH 8 NaPi	9.8	33.6
12	CoO‖	0.0032	0	pH 8 NaPi	0	0

* Same theoretical cobalt concentration as 0.0032 mM **1**; † Same solid mass as 0.0032 mM **1**; ‡ a mixed buffer of 30 mM NaPi and 30 mM phthalic acid at pH 6.2 was used; § a 1 mM stock solution in 30 mM pH 8 NaPi was left for 72 hours before use; ‖ not soluble, suspension obtained after 10 minutes of sonication.

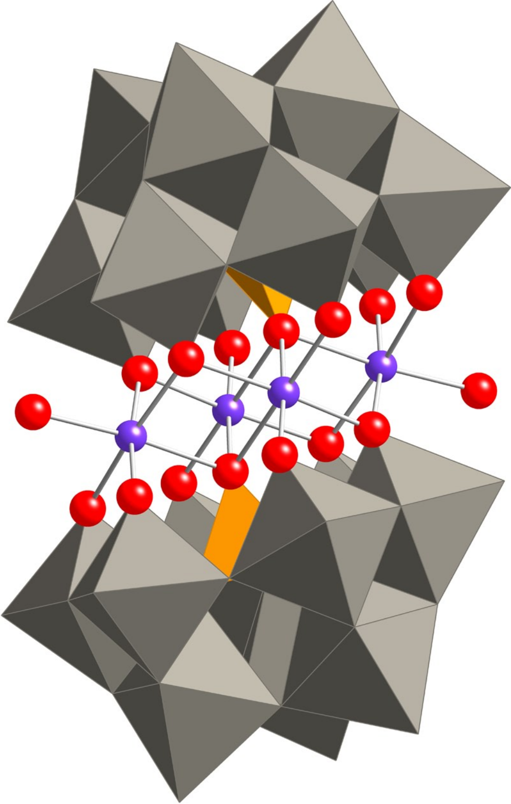

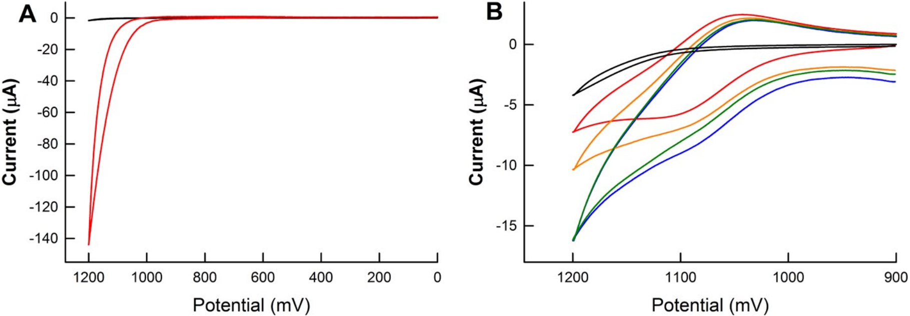
A
B
Current (μA)
0
-20
-40
-60
-80
-100
-120
-140
1200
1000
800
600
400
200
0
Potential (mV)
Current (μA)
0
-5
-10
-15
1200
1100
1000
900
Potential (mV)

www.sciencemag.org/cgi/content/full/science.1185372/DC1

Supporting Online Material for

A Fast Soluble Carbon-Free Molecular Water Oxidation Catalyst Based on Abundant Metals

Qiushi Yin, Jeffrey Miles Tan, Claire Besson, Yurii V. Geletii, Djamaladdin G. Musaev, Aleksey E. Kuznetsov, Zhen Luo, Ken I. Hardcastle, Craig L. Hill*

*To whom correspondence should be addressed. E-mail: chill@emory.edu

Published 11 March 2010 on *Science* Express
DOI: 10.1126/science.1185372

This PDF file includes:

Supporting online material (SOM) for

A fast soluble carbon-free molecular water oxidation catalyst based on abundant metals

Qiushi Yin,[1] Jeffrey Miles Tan,[1] Claire Besson,[1,2] Yurii V. Geletii,[1] Djamaladdin G. Musaev,[1] Aleksey E. Kuznetsov,[1] Zhen Luo,[1] Ken I. Hardcastle,[1] Craig L. Hill[1]

[1]Department of Chemistry, Emory University, Atlanta, GA 30322, USA.
[2]Institut Parisien de Chimie Moléculaire, UMR CNRS 7201, UPMC Univ. paris 06, Case 42, 4 place Jussieu, 75005 Paris, France.

Materials and Methods

Synthesis of POMs

(a) Synthesis of compound 1

The preparation of **Na$_{10}$-1** is derived from that of **K$_{10}$-1** reported in literature (*S1*). A higher yield preparation of **K$_{10}$-1** was reported by Finke *et al* (*S2*). To synthesize **Na$_{10}$-1**, $Na_2WO_4\cdot 2H_2O$ (35.62 g, 0.108 mol), $Na_2HPO_4\cdot 7H_2O$ (3.22 g, 0.012 mol), and $Co(NO_3)_2\cdot 6H_2O$ (6.98 g, 0.024 mol) were mixed in 100 mL water. After adjusting the pH from 9 to 7, this purple suspension was then refluxed at 100°C for two hours. A dark purple solution resulted within minutes of heating. After reflux, the solution was saturated with NaCl and allowed to cool to room temperature. The resulting purple crystals were collected, quickly washed with approximately 30 mL of water, and recrystallized from hot water (35% mass yield based on Co). Thermogravimetric analysis gave 27 water molecules of hydration (Fig. S10). FT/IR (cm^{-1}): 1037 (m), 939 (m), 882 (w), 767 (w) (Fig. S6). UV-Vis (H_2O, pH 3.5 to 9): λ_{max}, 579 nm (ε_{579} = 330 M^{-1} cm^{-1}) (Fig. S3). ^{31}P-NMR: 1855 ppm, $\Delta\nu_{1/2}$ = 400 Hz; Elemental analysis calculated (%) for $Na_{10}[Co_4(H_2O)_2(PW_9O_{34})_2]\cdot 27H_2O$: Co, 4.33; Na, 4.22; P, 1.14; W, 60.76. Found: Co, 4.49; Na, 4.24; P, 1.06; W, 58.7.

(b) Synthesis of compounds 2-8

The preparation of compounds **2-8** were performed according to the published literature (*S3*-*S9*). Their purity was confirmed by IR.

X-ray diffraction

The complete datasets for **Na$_{10}$-1** were collected at Emory University. A suitable crystal of **Na$_{10}$-1** was coated with Paratone N oil, suspended in a small fiber loop and placed in a cooled nitrogen gas stream at 173 K on a Bruker D8 APEX II CCD sealed tube diffractometer with graphite monochromated MoK_α (0.71073 Å) radiation. Data were measured using a series of combinations of phi and omega scans with 10 s frame exposures and 0.5^o frame widths. Data collection, indexing and initial cell refinements were all carried out using APEX II software (*S10*). Frame integration and final cell refinements were done using SAINT software (*S11*). The final cell parameters were determined from least-squares refinement on 9978 reflections.

The structure was solved using Direct methods and difference Fourier techniques (SHELXTL, V6.12) (*S12*). Only the Co, Na and W atoms were refined anisotropically; no hydrogen atoms were included in the final structure. Scattering factors and anomalous dispersion corrections are taken from the *International Tables for X-ray Crystallography* (*S13*). Structure solution, refinement, graphics and generation of publication materials were performed by using SHELXTL, V6.12 software. Additional details of data collection and structure refinement are given in Table S1.

Analysis of O_2 content using gas chromatography (GC)

A round-bottom flask with a total volume of ~17 mL was used to hold 8 mL of aqueous $[Ru(bpy)_3]^{3+}$ solution. A thick-wall tube was used to hold 2 mL of the catalyst in buffered solution. Both containers were capped with a rubber stopper and extensively deaerated by bubbling argon gas through the solution for over 10 minutes. The 2 mL solution in the thick-wall tube was then quickly transferred into the round-bottom flask using a cannula. This affords 10 mL of reaction solution. We report the species concentrations in this solution. A fully deaerated 250 μL Hamilton gas-tight syringe was used to withdraw a sample of the gas from the reaction vessel headspace. Aliquots (100 μL) of this gas were immediately injected into a Hewlett-Packard 5890 gas chromatograph fitted with a thermal conductivity detector for analysis. For timed reactions, a stopwatch was used to measure the time elapsed from the time of solution transfer via cannula to the time at which gas was withdrawn from the headspace. TOF for **1** is given as the final TON divided by the time elapsed.

Calibration of this system was performed using the exact same procedures substituting the reaction solutions with water. Four reference volume of O_2 were used in constructing a multipoint calibration slope. After mixing, 0 μL, 23.5 μL, 47 μL, or 70.5 μL of pure O_2 (corresponding to 0, 1, 2, or 3 μmol O_2) were injected into the headspace of the reaction vessel. The reaction vessel was shaken to allow equilibration of O_2 between gas and aqueous phases. The retention times of oxygen and nitrogen were separated by approximately 20 seconds. The oxygen peak was seen first a little under 1 minute. Contamination from air was minimal (< 0.07 μmol O_2 for the chemical oxidation of water) and accounted for by subtracting half of the nitrogen peak area from the total oxygen peak area. This is a conservative estimate, as the gas chromatograph gives an oxygen to nitrogen ratio of 1 : 2.8 for a sample of air. The amount of O_2 was plotted against the integration area for the adjusted oxygen peak. A linear correlation between the two was found and the slope was used as the conversion factor for the quantification of O_2 – yield in future experiments. Three data points were taken for each reference volume and the average O_2 peak area was used in the calibration, giving a Pearson r-value of > 0.99.

Cyclic voltammetry

Cyclic voltammograms (CVs) were obtained at room temperature in buffered solutions using BAS CV-50W voltammetric analyzer. An Ag/AgCl (3 M NaCl) reference electrode from BAS was calibrated using the $[Fe(CN)_6]^{3-}/[Fe(CN)_6]^{4-}$ couple, for which accurate published data are available (*S14*). On the basis of this calibration, potentials in the CV are reported relative to the NHE by the addition of 200 mV to the BAS electrode values.

UV-Visible spectroscopy

All UV-Vis spectroscopy was performed with an Agilent 8453 spectrometer at 25 °C using a quartz cell with a 1 cm pathlength. The UV-Vis spectroscopy of **1** is shown in Fig. S3. No changes in its spectrum were observed during any of the hydrolytic stability studies.

^{31}P NMR

The ^{31}P (243 MHz) NMR spectra were obtained at 300 K in 5 mm o. d. tubes on a Unity Plus 600 spectrometer equipped with a Varian 600 SW/PF6 probehead. The chemical shifts are given with respect to 85 % H_3PO_4. Acquisition parameters are as follows: pulsewidth 4 μs (~40° flip angle), time domain window 100 kHz (412 ppm), 1500 (for diluted solutions) or 3000 (for concentrated solutions) points, resulting in acquisition times of 7.5 or 15 μs respectively

Effect of bpy on cobalt oxide/hydroxide formation at high pH

Adding a few drops of 1 M aqueous NaOH to a 1 mM solution of $Co(NO_3)_2$ turned the solution slightly blue. This color quickly disappears and a white precipitate was observed, indicating the formation of cobalt oxide/hydroxide aggregate. When 6 equivalents of bpy is added to a 1 mM solution of $Co(NO_3)_2$, a yellow solution results (Fig. S2). Adding aqueous NaOH to this solution does not yield any precipitate. This further demonstrates that bpy prevents the formation of catalytically active cobalt oxide/hydroxides.

Characterization of the post-catalysis solution

(a) Preparation of solution for ^{31}P-NMR

Tris(2,2'-bipyridyl)triperchlororuthenium(III) ($[Ru(bpy)_3]^{3+}$, 11.0 mg, 11.3 μmol) was dissolved in D_2O (15 mL). A separate solution containing **1** (0.075 mM) and NaPi (0.16 M, pH 8.0) was prepared in in 1:5 D_2O/H_2O. A 2 mL aliquot of the latter solution was then added to 8 mL of the former solution, resulting in 0.6 mM $[Ru(bpy)_3]^{3+/2+}$, 0.015 mM **1**, and 32 mM NaPi dissolved in 5:1 D_2O/H_2O. After the reaction was completed, $Na[BPh_4]$ (18 mg, 52.6 μmol) was added to this solution. The resulting light yellow precipitate was filtered off using a micro-filter. The completely colorless filtrate was used for ^{31}P NMR (Fig. S5).

(b) Re-isolation of catalytically active species

$[Ru(bpy)_3](ClO_4)_3$ (276.7 mg, 0.285 mmol) was dissolved in water (152 mL). A separate aqueous solution of **1** (0.016 mM **1** in 0.153 M NaPi at pH 8.0, 38 mL) was then added. After reaction completion, the solution was concentrated via evaporation. When the solution volume was approximately 50-60 mL, tris(2,2'-bipyridyl)dichlororuthenium(II) hexahydrate ($[Ru(bpy)_3]^{2+}$, 150 mg, 0.20 mmol) was added to this solution, inducing the formation of a light yellow precipitate. The yellow precipitate (1.1 mg) was collected by centrifugation and dried under vacuum, characterized using FT-IR spectroscopy (Fig. S6) and tested for WOC activity.

Computational procedures

All calculations were performed using the Turbomole program (*S15*). The geometries of these species were optimized with C_i-symmetry constraints at the RI-PBE level. In these calculations we use the triple zeta plus polarization (TZVP) basis sets (*S16*) for all atoms together with relativistic effective core potentials for Co and W from the Stuttgart group (*S17*). Solvent effects were taking into account using the Conductor-like Screening Model (COSMO) (*S18*) with water as a solvent ($R_{solvent}$ = 1.30 Å) and the following atomic radii in Å: O, 1.720; H, 1.300; Si, 2.458; 2 Co, W, 2.2225. Computational studies of the geometry and electronic structure of **1** at its ground high-spin state provide an excellent agreement with previous experimental data (*S1*) as well as our data on the geometry of this species (Fig. S9). The frontier orbital analysis (HOMOs and LUMOs) indicates that HOMO orbitals are close in energy: the calculated energy gap between the HOMO and HOMO-3 orbitals (Fig. S8) is 0.24 eV. The same picture is true for the LUMO orbitals: the calculated energy difference between LUMO and LUMO+3 orbitals is 0.55 eV. The HOMO-LUMO energy gap is calculated to be a 1.22 eV. Thus, HOMOs and LUMOs of **1** (which are the Co_4O_4 core and WO bonding and antibonding orbitals) are well separated and clustered, respectively.

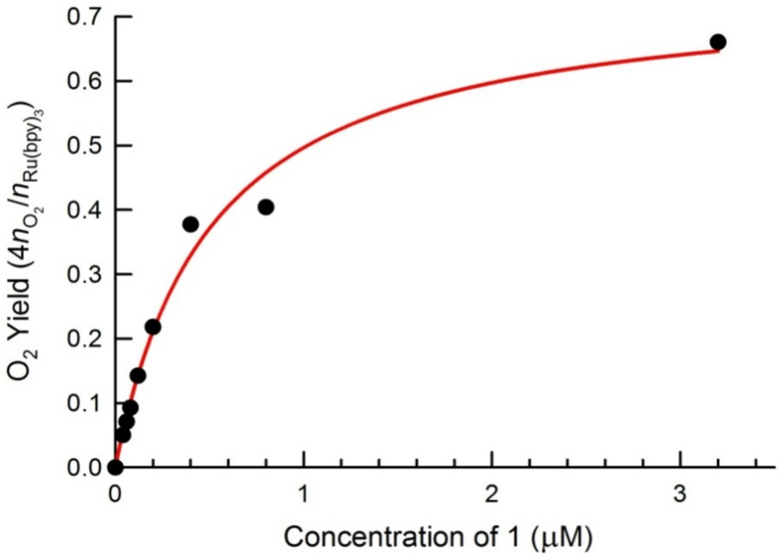

Fig. S1. The O_2-yield as defined in Table 1 versus the concentration of **1** (solid circles) and its hyperbolic fit (red line), Pearson correlation coefficient is 0.99. Reactions took place in 30 mM NaPi buffer, initial pH 8.0, 1.5 mM $[Ru(bpy)_3]^{3+}$, r.t. The hyperbolic fit is consistent with a simplified reaction mechanism in equations 1S-2S using the steady-state approximation for the catalyst concentration and assumptions that $r_{1S} = 4k_1[\mathbf{1}]\,f([Ru(bpy)_3]^{3+})$ and $r_{2S} = k_2\,g([Ru(bpy)_3]^{3+}, Ru(bpy)_2(bpy'))]^{2+})$, where (bpy') is oxidatively damaged bpy:

$$4[Ru(bpy)_3]^{3+} + 2H_2O \xrightarrow[\mathbf{1}]{k_1} 4[Ru(bpy)_3]^{2+} + O_2 + 4H^+ \quad (1S)$$

$$[Ru(bpy)_3]^{3+} \xrightarrow{k_2} [Ru(bpy)_2(bpy')]^{2+} \quad (2S)$$

A simple derivation results in a hyperbolic function of y versus $[\mathbf{1}]$, equation 3S:

$$y = \frac{n_{O_2}}{\frac{1}{4}n_{Ru(bpy)_3}} = \frac{\int_0^\infty 4k_1[\mathbf{1}]\,f([Ru(bpy)_3]^{3+})dt}{\int_0^\infty 4k_1[\mathbf{1}]\,f([Ru(bpy)_3]^{3+})dt + \int_0^\infty k_2 g([Ru(bpy)_3]^{3+},[Ru(bpy)_3]^{2+})dt}$$

$$y = \frac{4k_1[\mathbf{1}]\int_0^\infty f([Ru(bpy)_3]^{3+})dt}{4k_1[\mathbf{1}]\int_0^\infty f([Ru(bpy)_3]^{3+})dt + k_2\int_0^\infty g([Ru(bpy)_3]^{3+},[Ru(bpy)_3]^{2+})dt} = \frac{[\mathbf{1}]}{[\mathbf{1}] + \frac{k_2\int_0^\infty g([Ru(bpy)_3]^{3+},[Ru(bpy)_3]^{2+})dt}{4k_1\int_0^\infty f([Ru(bpy)_3]^{3+})dt}}$$

$$y = \frac{4n_{O_2}}{n_{Ru(bpy)_3}} = \frac{[\mathbf{1}]}{[\mathbf{1}] + C} \qquad (3S)$$

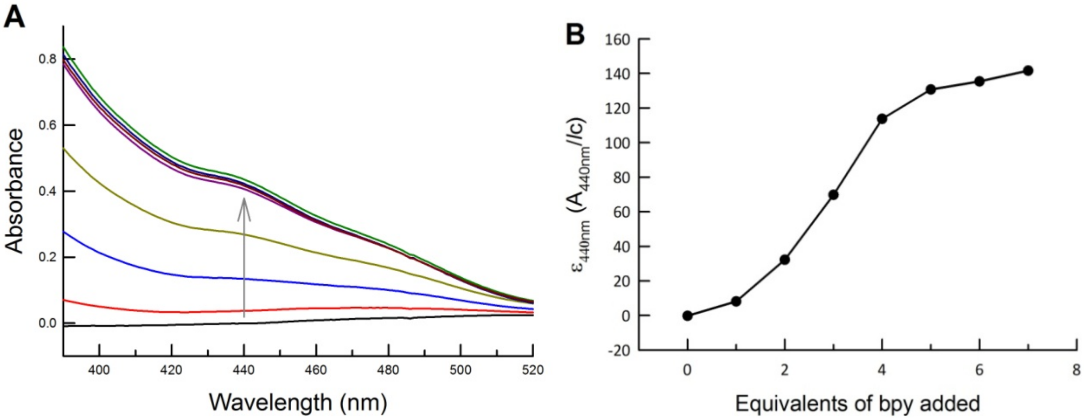

Fig. S2. (A) UV-Visible spectroscopy indicating the appearance of the bpy cobalt complex with increasing amounts of added bpy. A 5 mM solution of $Co(NO_3)_2$ is titrated using a 50 mM solution of bpy. **(B)** The extinction coefficient (M^{-1} cm^{-1}) at 440 nm versus the equivalents of bpy added (corrected for a 1/10 dilution factor after each addition).

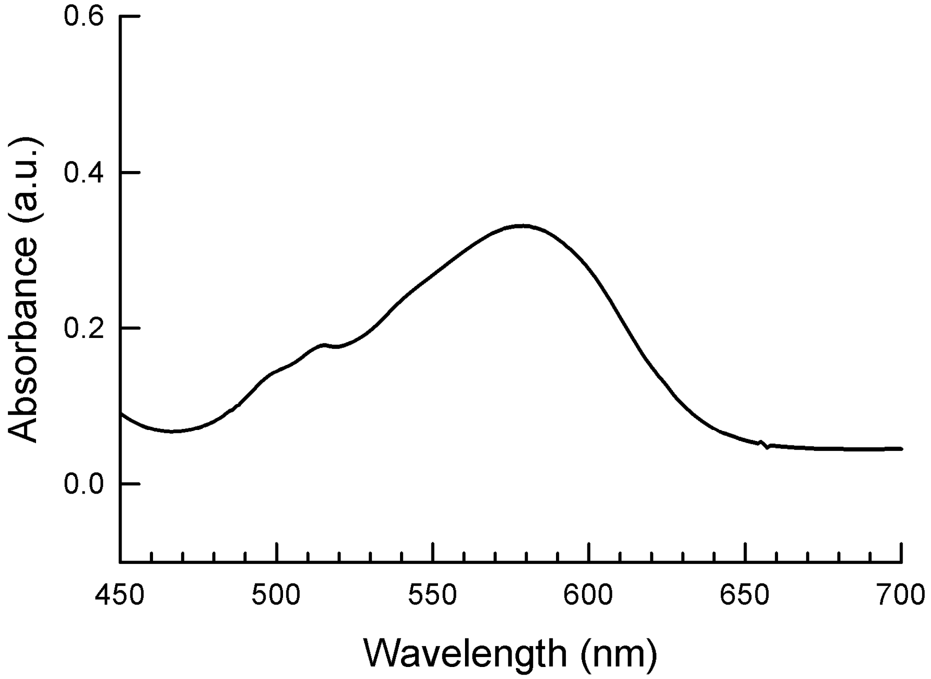

Fig. S3. UV-Visible spectroscopy of 1 mM **1** in 30 mM pH 8 NaPi buffer. The spectrum does not change with variation in solution age and solution pH. The calculated extinction coefficient at λ_{max} (579 nm) is ε_{579} = 330 M^{-1} cm^{-1}.

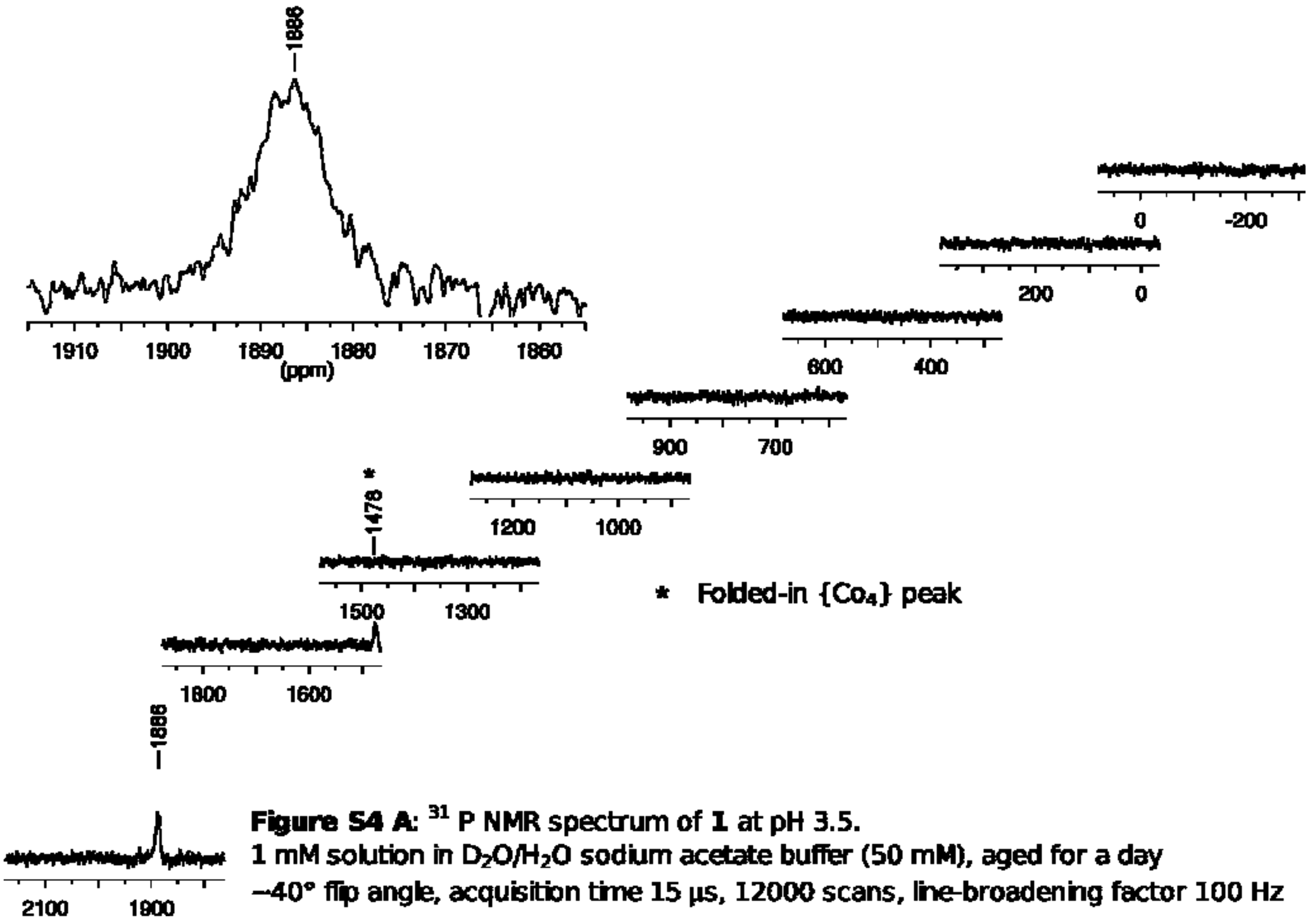

Figure S4 A: ^{31} P NMR spectrum of **1** at pH 3.5.
1 mM solution in D_2O/H_2O sodium acetate buffer (50 mM), aged for a day
~40° flip angle, acquisition time 15 μs, 12000 scans, line-broadening factor 100 Hz

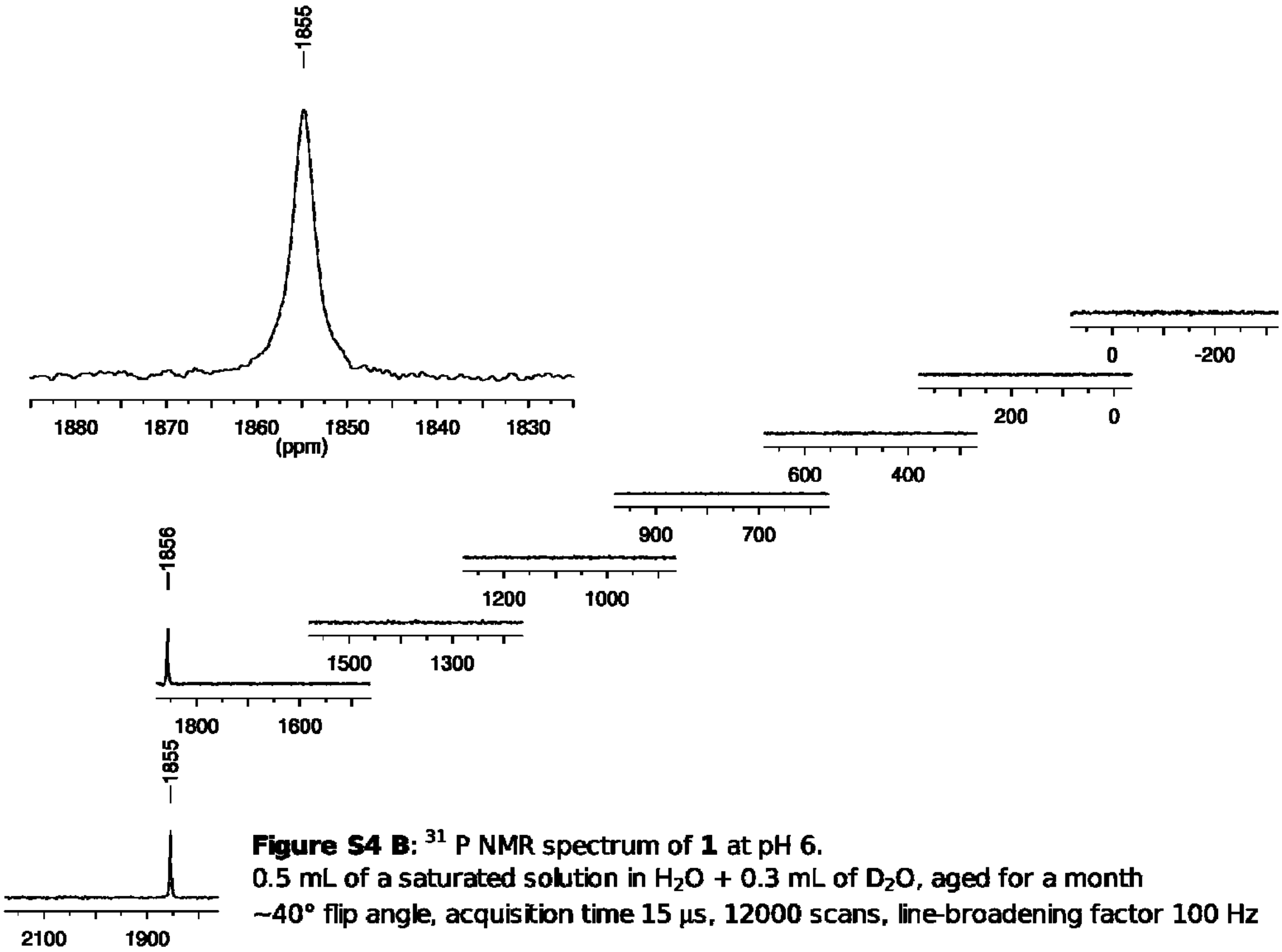

Figure S4 B: ^{31} P NMR spectrum of **1** at pH 6.
0.5 mL of a saturated solution in H_2O + 0.3 mL of D_2O, aged for a month
~40° flip angle, acquisition time 15 µs, 12000 scans, line-broadening factor 100 Hz

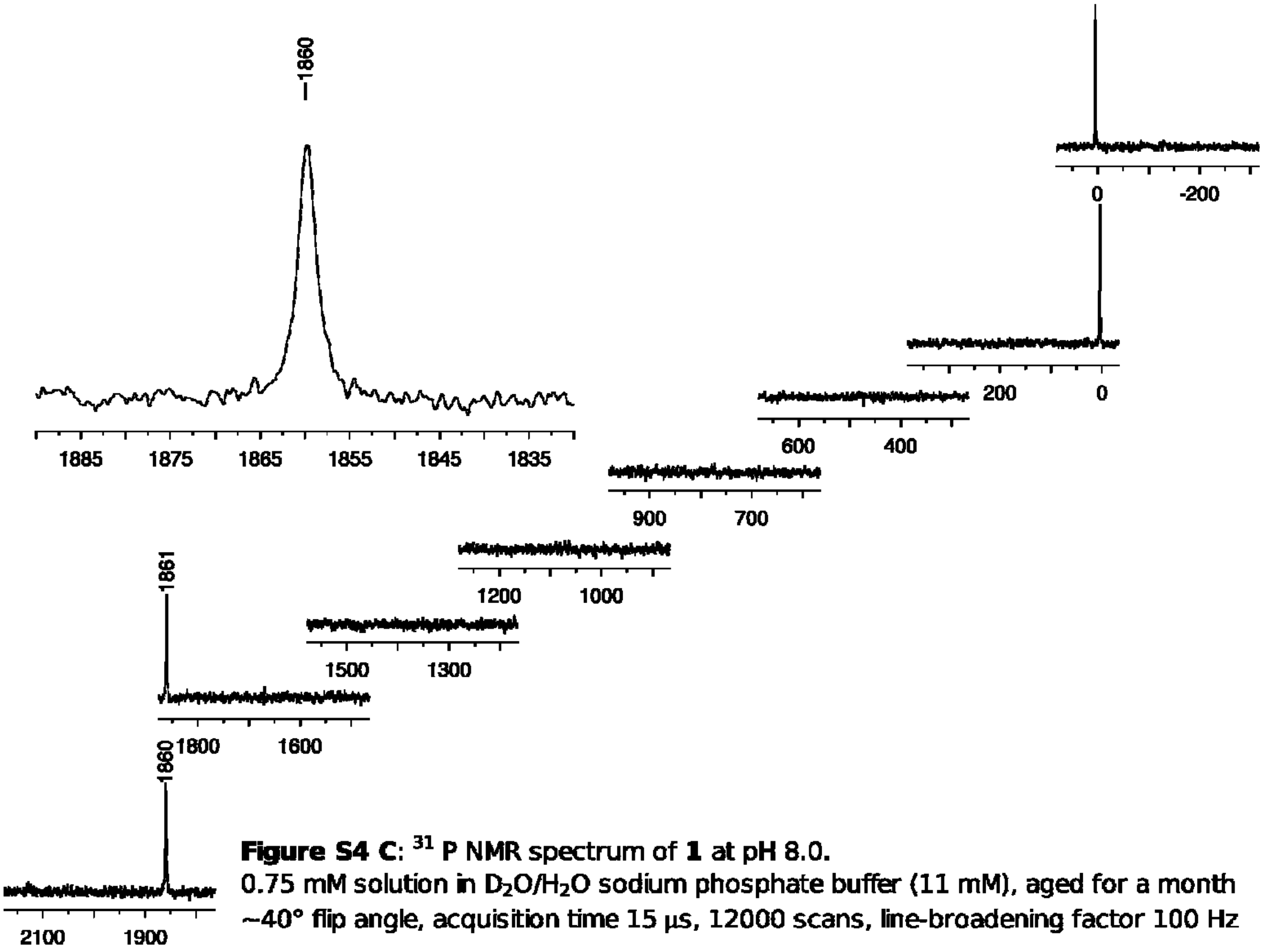

Figure S4 C: ^{31}P NMR spectrum of **1** at pH 8.0.
0.75 mM solution in D_2O/H_2O sodium phosphate buffer (11 mM), aged for a month
~40° flip angle, acquisition time 15 μs, 12000 scans, line-broadening factor 100 Hz

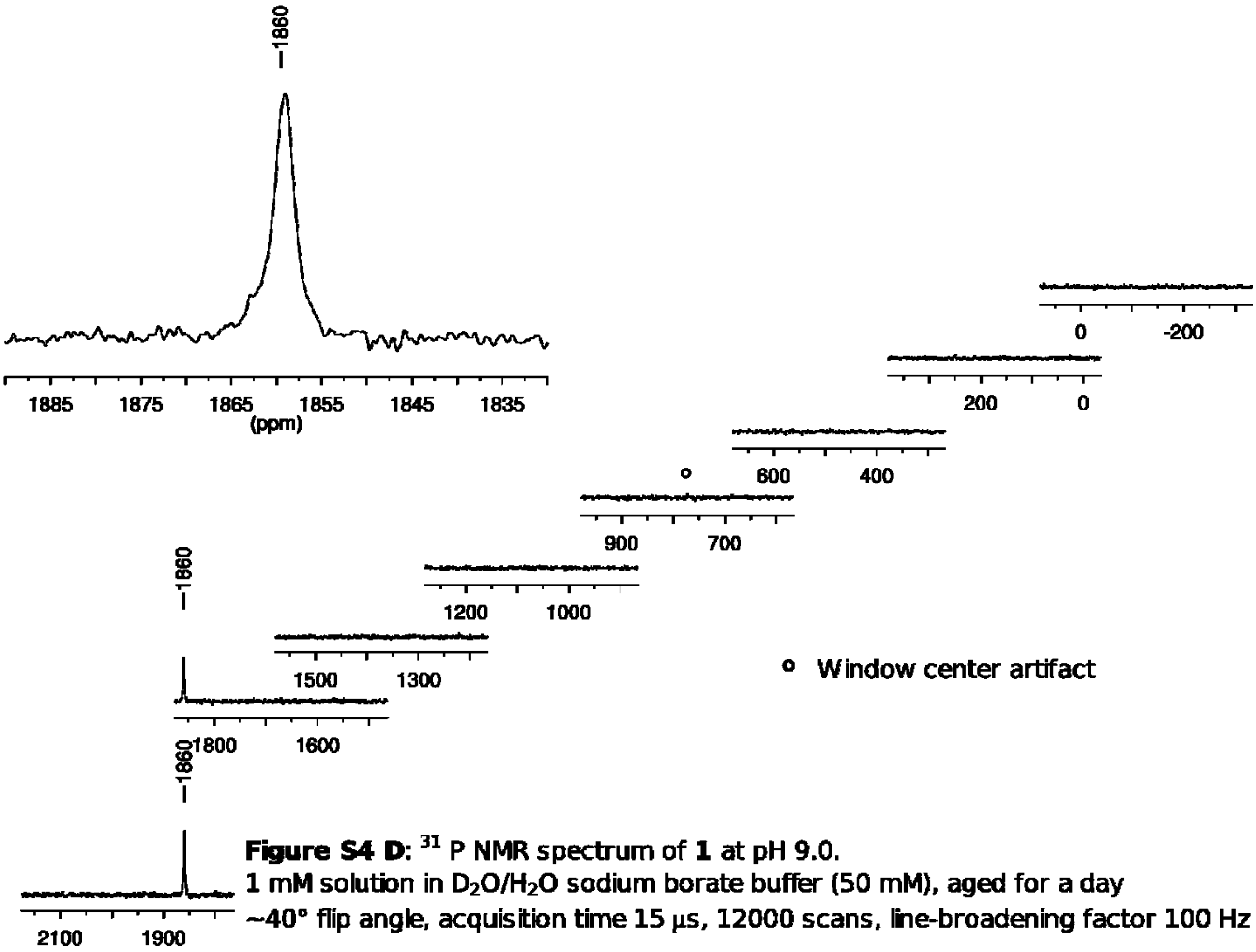

Figure S4 D: ^{31} P NMR spectrum of **1** at pH 9.0.
1 mM solution in D_2O/H_2O sodium borate buffer (50 mM), aged for a day
~40° flip angle, acquisition time 15 µs, 12000 scans, line-broadening factor 100 Hz

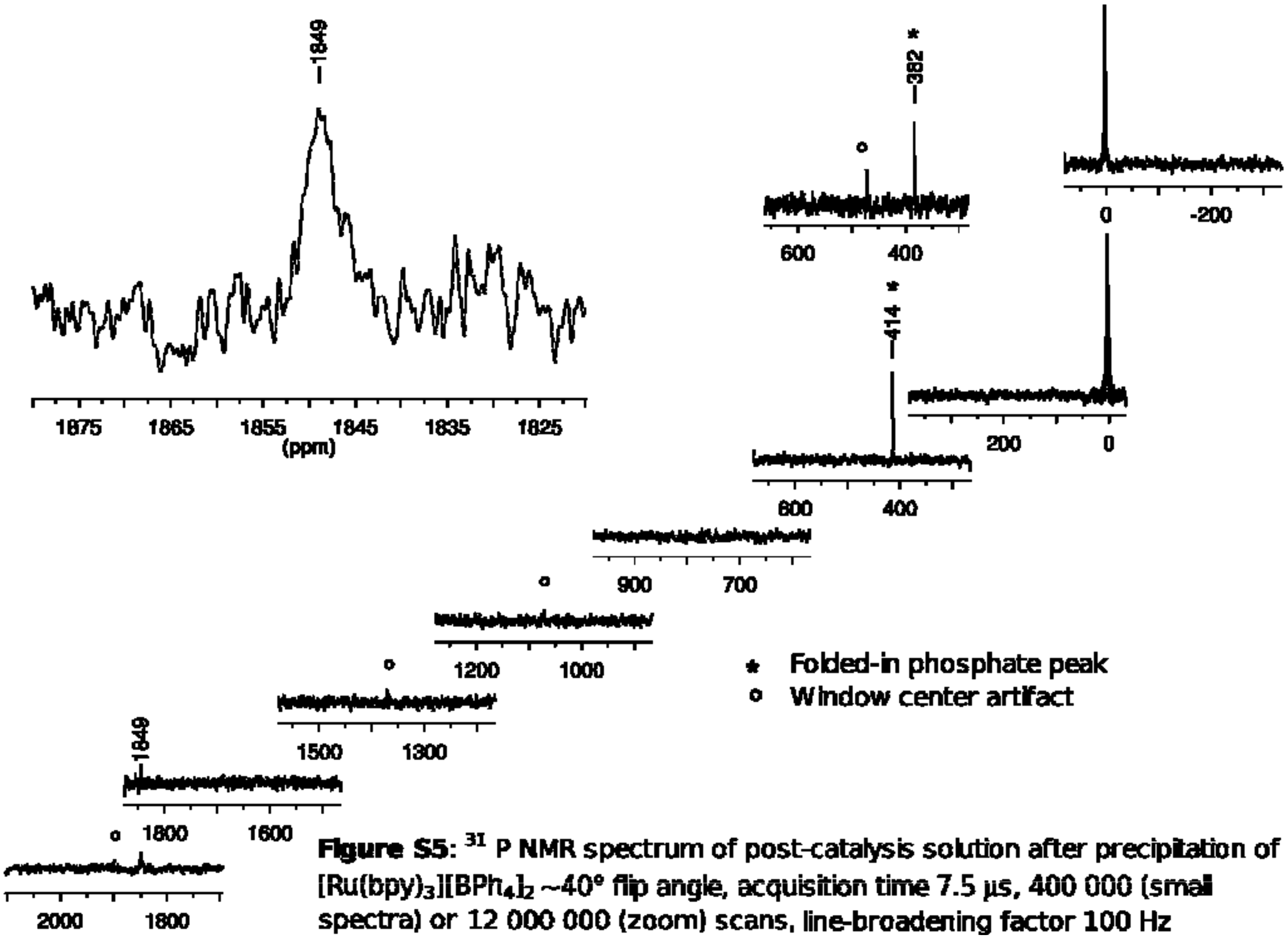

Figure S5: ^{31}P NMR spectrum of post-catalysis solution after precipitation of [Ru(bpy)$_3$][BPh$_4$]$_2$ ~40° flip angle, acquisition time 7.5 µs, 400 000 (small spectra) or 12 000 000 (zoom) scans, line-broadening factor 100 Hz

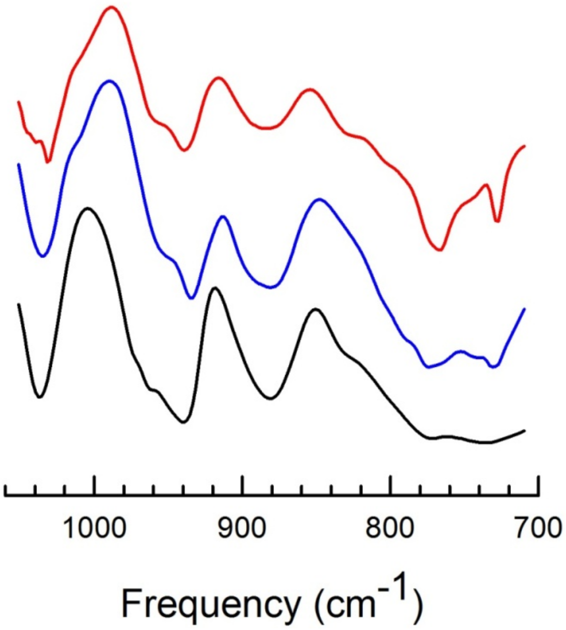

Fig. S6. FT-Infrared spectrum of **Na_{10}-1** (black), the light-yellow precipitate re-isolated from a "post-chemical reaction" solution (red), and the dark-yellow precipitate obtained from mixing two concentrated solutions of **Na_{10}-1** and $[Ru(bpy)_3]^{2+}$ (blue). All FT-IR spectroscopy were performed using 1 wt% sample in KBr pellet. All three spectra show the characteristic P-O stretching (1037 cm^{-1}), terminal W-O stretching (939 cm^{-1}), and W-O-W bending (882 and 767 cm^{-1}) bands.

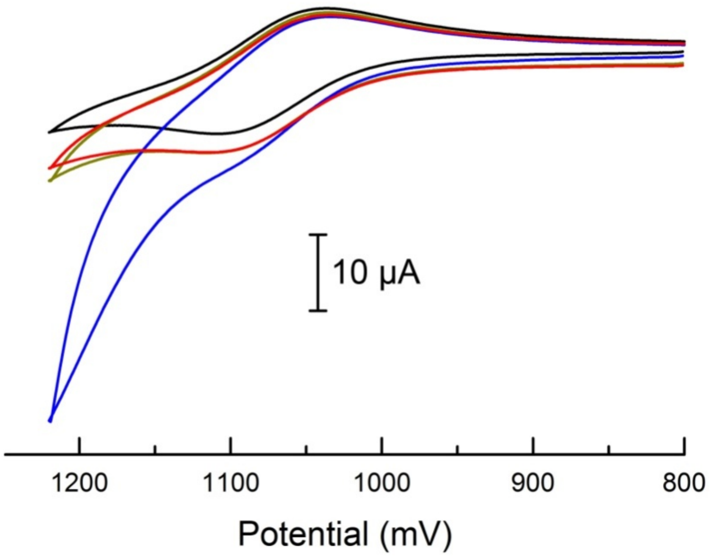

Fig. S7. Cyclic voltammograms: 0.857 mM $[Ru(bpy)_3]^{2+}$ (black); a "post-chemical reaction" solution containing 0.857 mM $[Ru(bpy)_3]^{2+}$ and 0.0128 mM $Co(NO_3)_2$ (red); an "unreacted" model solution containing 0.857 mM $[Ru(bpy)_3]^{2+}$ and 0.0128 mM $Co(NO_3)_2$ (blue); or 0.0064 mM $Co(NO_3)_2$ (yellow). The solutions are buffered using 60 mM NaPi, pH 8, scan rate 25 mV/s.

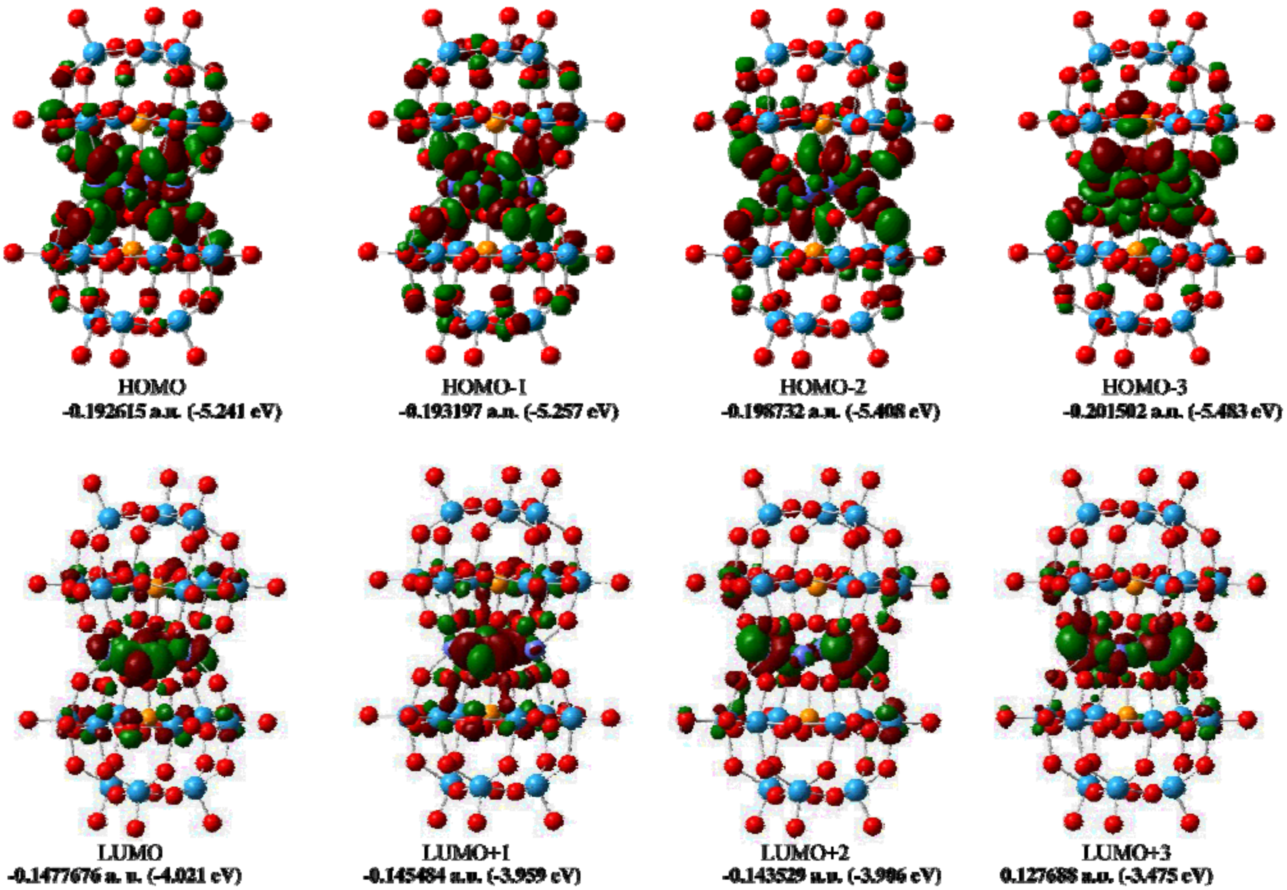

Fig. S8. RI-PBE/PCM calculated HOMO's and LUMO's of **1**, ${}^{13}A_g$, with their orbital energies.

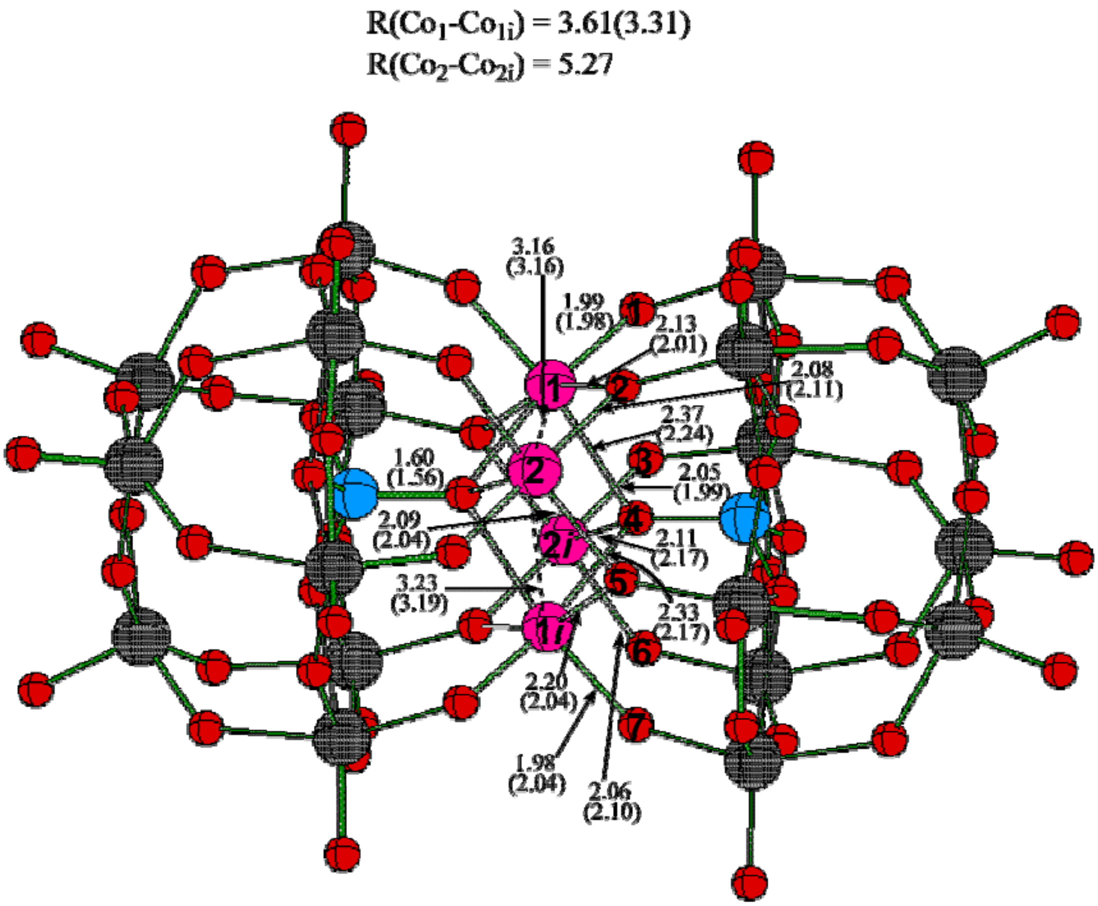

Fig. S9. Calculated cobalt-core geometry parameters (at the PBE/TZVP level) of the high-spin ground state of **1** compared with experimental data (in parentheses).

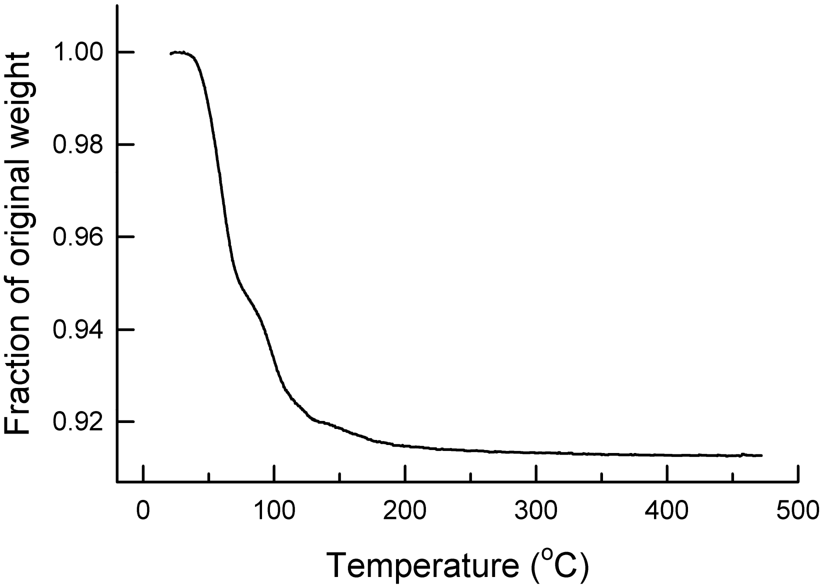

Fig. S10. Thermogravimetric Analysis (TGA) of crystalline **Na$_{10}$-1**. The weight loss observed (9%) is attributed to waters of hydration. Given that $Na_{10}Co_4(H_2O)_2P_2W_{18}O_{68}$ has a formula weight of 4962, there are approximately 27 waters of hydration as determined by TGA.

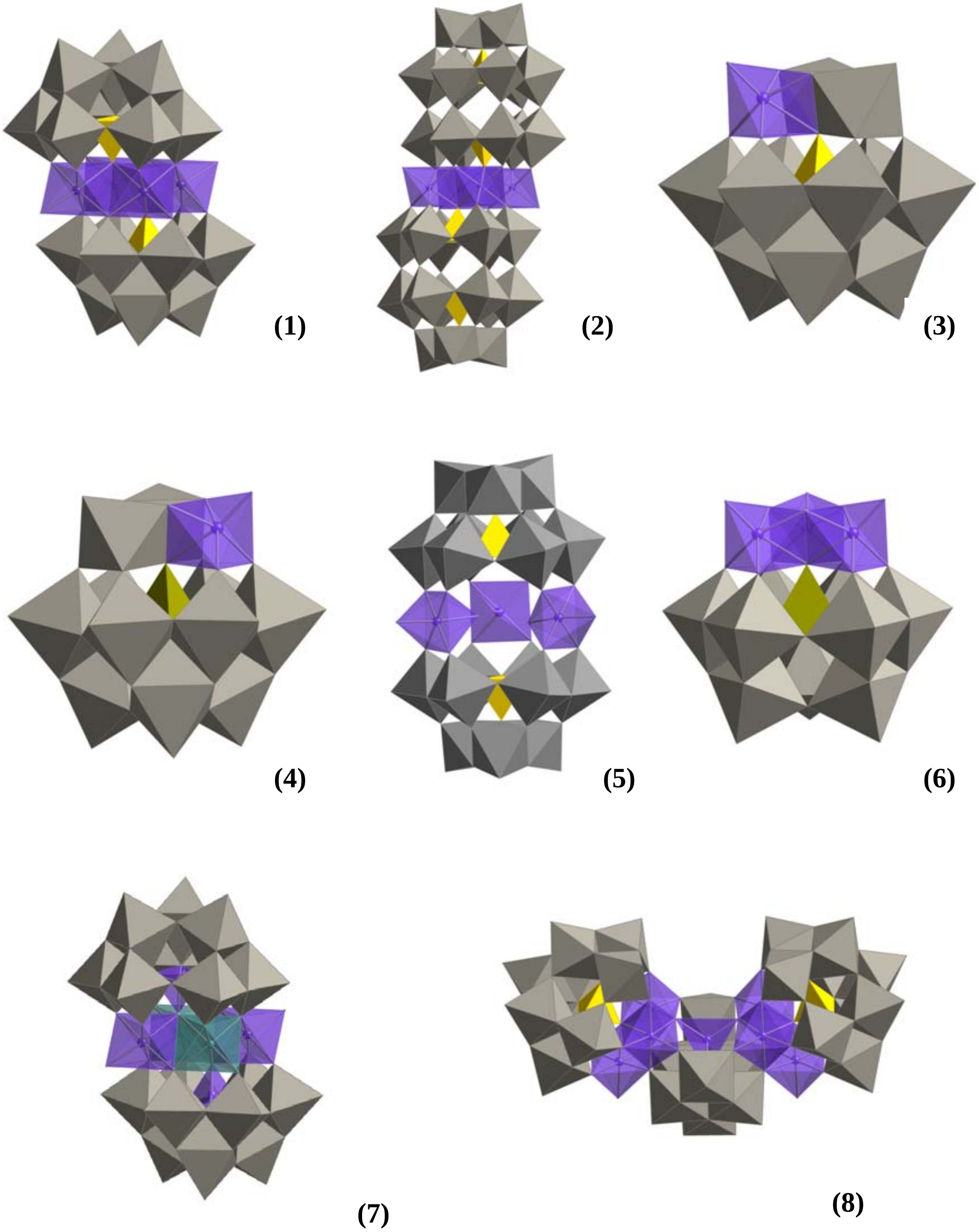

(1) (2) (3)

(4) (5) (6)

(7) (8)

Fig. S11 A. Polyhedral representation of the cobalt-containing polytungstate complexes **1-8**. Purple: Co; Grey: WO_6; Yellow: PO_4; Green: SiO_4; Blue: Co and W are disordered in the two positions.

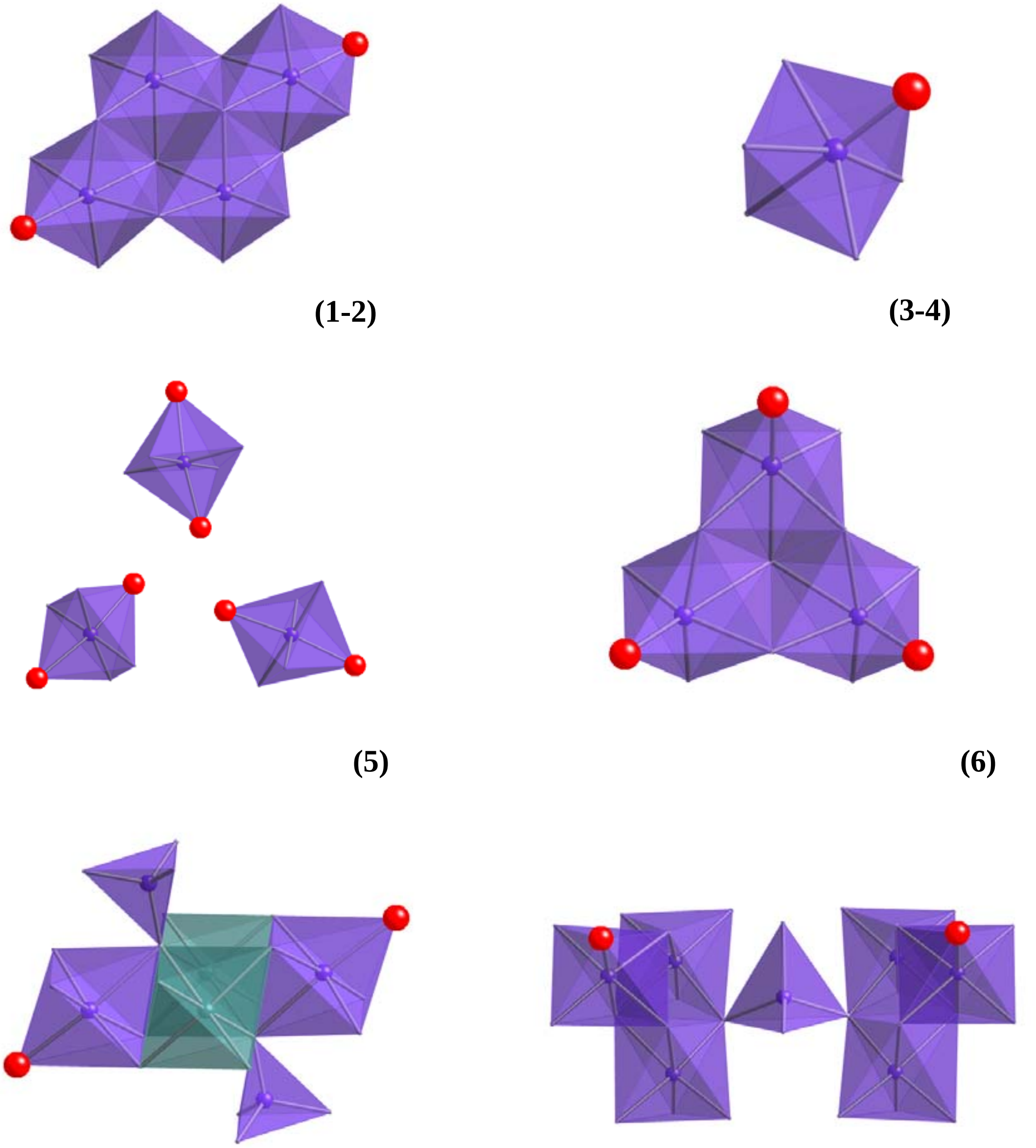

(1-2) **(3-4)**

(5) **(6)**

(7) **(8)**

Fig. S11 B. Polyhedral representation of the Co core structures of the cobalt-containing polytungstate complexes, **1-8**. Purple ball: Co; Red ball: Terminal O; Blue ball: Co and W disordered in the two positions. All bridging oxygen atoms were omitted.

Table S1. Crystal data and refinement parameters for the X-ray structure of **Na_{10}-1**

complex	**Na_{10}-1**
molecular formula	$Na_{10}Co_4O_{98.66}P_2W_{18}$
formula wt. (g mol^{-1})	5415.42
temperature (K)	172(2)
radiation (λ, Å)	0.71073
crystal system	Triclinic
space group	*P-1*
a (Å)	11.539(3)
b (Å)	12.807(4)
c (Å)	17.259(5)
α (°)	98.019(4)
β (°)	106.639(4)
γ (°)	111.205(4)
Volume (Å^3)	2192.3(11)
Z	1
μ (mm^{-1})	24.451
F(000)	2369
crystal size (mm^3)	0.38 x 0.32 x 0.20
reflections collected	40531
independent reflections	11692 [R(int) = 0.0469]
absorption correction	semi-empirical from equivalents
refinement method	full-matrix least-squares on F^2
goodness-of-fit on F^2	1.078
final R indices	$R1^a = 0.0814$
[$R > 2\sigma$ (I)]	$wR2^b = 0.2374$
R indices (all data)	$R1^a = 0.0951$, $wR2^b = 0.2643$

$^a R_1 = \Sigma||F_o| - |F_c|| / |F_o|$

$^b wR_2 = \{\Sigma[w(F_o^2 - F_c^2)^2] / \Sigma[w(F_o^2)^2]\}^{0.5}$

SOM References

S1. T. J. R. Weakley, H. T. Evans, J. S. Showell, G. F. Tourné, C. M. Tourné, *J. Chem. Soc., Chem. Commun.*, 139 (1973).

S2. R. G. Finke, M. W. Droege, P. J. Domaille, *Inorg. Chem.* **26**, 3886 (1987).

S3. R. G. Finke, M. W. Droege, *Inorg. Chem.* **22**, 1006 (1983).

S4. T. J. R. Weakley, *J. Chem. Soc., Dalton Trans.*, 341 (1973).

S5. T. J. R. Weakley, S. A. Malik, *J. inorg. nucl. Chem.* **29**, 2935 (1967).

S6. W. H. Knoth, P. J. Domaille, R. D. Farlee, *Organometallics* **4**, 62 (1985).

S7. J. Liu *et al.*, *J. Chem. Soc., Dalton Trans.*, 1901 (1992).

S8. C. M. Tourné, G. F. Tourné, F. Zonnevijlle, *J. Chem. Soc., Dalton Trans.*, 143 (1991).

S9. J. M. Clemente-Juan *et al.*, *Inorg. Chem.* **43**, 2689 (2004).

S10. Bruker APEX 2, Bruker AXS Inc., Madison, Wisconsin, USA SAINT Version 6.45A (2003).

S11. Bruker SAINT, Bruker AXS Inc., Madison, Wisconsin, USA.

S12. G. M. Sheldrick, *Acta Cryst.* **A64**, 112 (2008).

S13. A. J. C. Wilson, *International Tables for X-ray Crystallography*. (Kynoch, Academic Publishers, Dordrecht, 1992), vol. C.

S14. R. E. Panzer, P. J. J. Elving, *Electrochem. Soc.* **119**, 864 (1972).

S15. R. Ahlrichs, M. Bär, M. Häser, H. Horn, C. Kölmel, *Chem. Phys. Lett.* **162**, 165 (1989).

S16. K. Eichkorn, F. Weigend, O. Treutler, R. Ahlrichs, *Theor. Chem. Acc.* **97**, 119 (1997).

S17. D. Andrae, U. Häussermann, M. Dolg, H. Stoll, H. Preuss, *Theor. Chim. Acta* **77**, 123 (1990).

S18. A. Klamt, G. Schüürmann, *J. Chem. Soc. Perkin Trans.* **2**, 799 (1993).